Analysis of the Effect of Differential-Mode and Common-Mode Impedance Matching on the Common-Mode Rejection Ratio of a Differential Electro-Optical Voltage Probe

Hrvoje Štimac*, Adrijan Barić*
*University of Zagreb Faculty of Electrical Engineering and Computing, Unska 3, 10000 Zagreb, Croatia
Tel: +385 (0)1 6129547, Fax: +385 (0)1 6129653, Email: hrvoje.stimac@fer.hr

***Abstract*—A differential electro-optical voltage probe is characterized. The two main parts of the probe circuit are the attenuator circuit and the laser diode. The probe circuit is characterized by measuring S-parameters. The probe circuit has a stable common-mode rejection ratio (CMRR) up to 4 GHz, with a quick drop at higher frequencies. The probe circuit performance is simulated by combining the individual attenuator and laser characteristics connected in cascade. The differential-mode and common-mode signal propagation is analyzed in terms of voltage and impedance matching. The impedance matching between the attenuator and the laser, in combination with their individual characteristics, determines the CMRR frequency characteristic of the probe circuit. By suppressing the common-mode signal propagation, relative to the differential-mode signal, an electro-optical system with a CMRR higher than the nominal CMRR of the laser diode can be designed.**

***Index Terms*—CMRR, common-mode, differential-mode, electro-optical probe, impedance matching.**

I. Introduction

Characteristics of a broadband differential electro-optical voltage probe are measured [1]. The probe circuit consists of two main parts, the attenuator circuit and the laser diode (Fig. 1). The attenuator is used to lower the input signal level in order not to overdrive the laser. The laser diode converts the measured radio frequency (RF) signal into an optical signal, which is transmitted to the photodetector. The laser is biased using a dedicated bias circuit. The probe circuit design is discussed in [2].

The characteristics of the differential electro-optical voltage probe are measured. The differential-mode component of the input signal presents the wanted signal, while the common-mode component presents the unwanted signal. The probe has a stable common-mode rejection ratio (CMRR) up to 4 GHz, which drops quickly at higher frequencies. The voltage attenuation ratio of the probe circuit is 125:1 (42 dB). The maximum input differential voltage amplitude is 25 V. The nominal differential-mode input impedance is 1092 Ω, and the nominal common-mode input impedance is 275 Ω.

Research typically focuses on overall external probe characteristics, with a desired CMRR of 30–40 dB up to 5 GHz [3], [4]. In contrast, the motivation for this paper is to understand the internal signal propagation through the probe circuit building blocks and its impact on the CMRR characteristics.

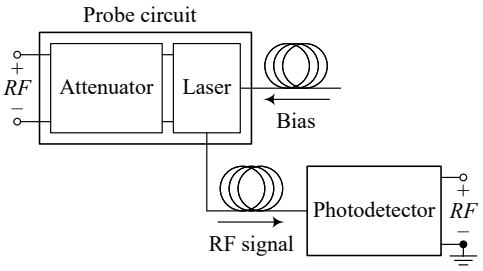

Fig. 1. Differential electro-optical voltage probe schematic.

In this paper, the differential-mode and common-mode signal propagation through the probe circuit is analyzed. The two main parts of the probe circuit, the attenuator and the laser, are analyzed separately. The performance of the probe circuit is simulated by combining the characteristics of these two building blocks. Based on the differential-mode and common-mode voltages and impedance matching between the attenuator and the laser, the CMRR characteristics of the probe are evaluated.

The probe characterization and simulation setup are presented in Section II. The signal propagation through the probe circuit is analyzed in Section III. The effect of the attenuator and laser characteristics on the CMRR of the probe circuit is discussed in Section IV. The conclusion is given in Section V.

II. Characterization and Simulation Setup

Three-port S-parameters of the probe circuit characterization structure shown in Fig. 2 are measured. The mea-

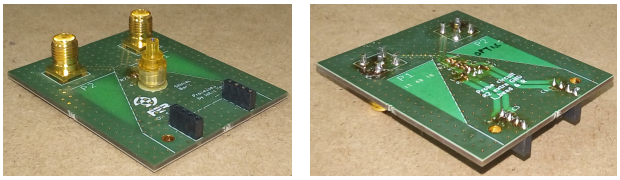

(a) Top side. (b) Bottom side.

Fig. 2. Probe circuit characterization structure.

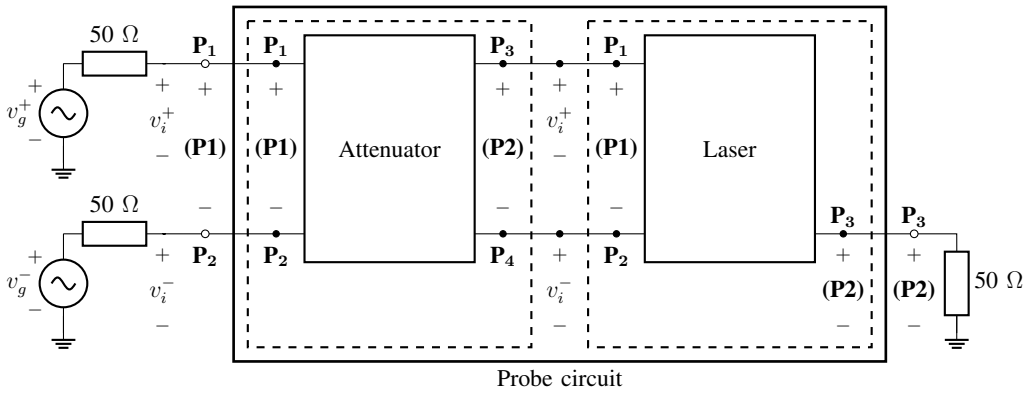

Fig. 3. Probe circuit represented as a cascade connection of the attenuator circuit and the laser.

surements are performed using a two-port vector network analyzer (VNA) [5], in the frequency range from 1 MHz to 8 GHz. The VNA output power is set to 0 dBm. The three-port standard single-ended S-parameters are de-embedded and converted to mixed-mode S-parameters [6], [7]. The CMRR of the probe circuit is calculated [8].

The schematic of the probe circuit characterization structure is shown in Fig. 3. In the probe circuit, the attenuator and the laser are connected in cascade. The goal is to simulate the performance of the probe circuit by combining the characteristics of the attenuator and the laser, that are characterized separately. Electromagnetic (EM) simulations of the attenuator structure, performed using a commercially available EM solver based on the finite element method (FEM) [9], are used in the probe circuit simulation. The mixed-mode S-parameters of the attenuator are calculated from the four-port standard single-ended S-parameter EM simulation results [6], [7]. The biased laser diode is measured separately. The VNA output power is set to –7 dBm, making sure that the laser operates in the linear region. Three-port S-parameter measurement results of the laser are used in the probe circuit simulation.

The probe circuit measurement and simulation results are compared in Fig. 4. The simulation results of the differential-mode transmission coefficient S_{sd21} show good matching to the measurement results. The simulation results match the general trend of the common-mode transmission coefficient S_{sc21} measurements. Taking into account the matching of the differential-mode and the common-mode signal transmission, the simulation results match the general trend of the common-mode rejection ratio measurements. The difference between the simulation and the measurement results varies between 3–5 dB. The simulated CMRR of the probe circuit remains above 20 dB up to 4.1 GHz. The fast drop in the measured CMRR at frequencies above 4.5 GHz is replicated by the probe circuit simulation results.

The differences between the simulation and measurement results are expected, because of the differences between the laser samples used, the components used in the attenuator circuit, the limitations of the attenuator EM simulations, as well as the coupling between the components of the probe circuit structure, which is not present when characterizing the parts individually.

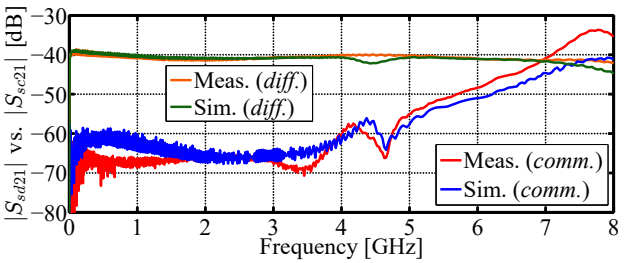

(a) Differential-mode and common-mode signal transmission.

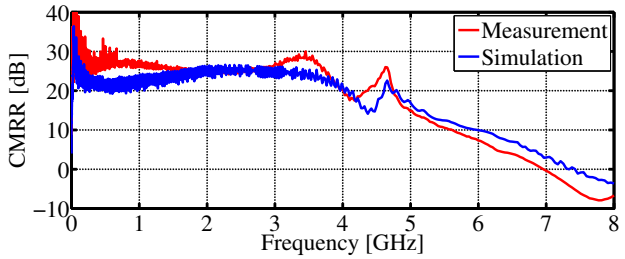

(b) Common-mode rejection ratio.

Fig. 4. Comparison of the measurement and the simulation of probe circuit. The magnitude of the differential-mode transmission coefficient S_{sd21}, the common-mode transmission coefficient S_{sc21}, and the common-mode rejection ratio (CMRR) are compared.

III. Signal Propagation

A. Probe Circuit Input Voltage

The probe circuit characterization setup is represented using the voltage sources v_g^+ and v_g^- with a 50 Ω internal impedance, and the 50 Ω termination load, shown in Fig. 5. In-phase generators $v_{c,g}^+$ and $v_{c,g}^-$ are used for the common-mode simulation. Counter-phase generators $v_{d,g}^+$ and $v_{d,g}^-$ are used for the differential-mode simulation. The generator voltages are set as follows:

$$v_{c,g}^+ = v_{c,g}^- = v_{d,g}^+ = v_{d,g}^- = 1 \text{ V}. \quad (1)$$

The common-mode voltage at the generator $v_{c,g}$ and the differential-mode voltage at the generator $v_{d,g}$ in the

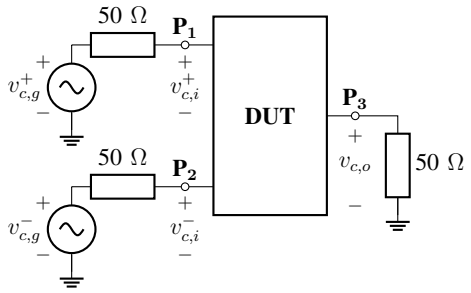

(a) Common-mode characterization setup.

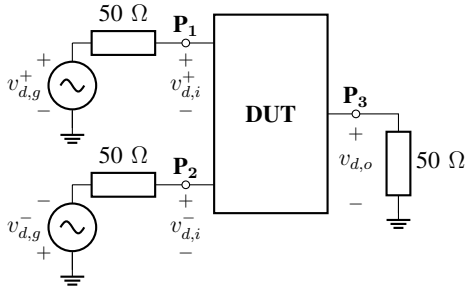

(b) Differential-mode characterization setup.

Fig. 5. Common-mode and differential-mode probe circuit characterization setup schematic.

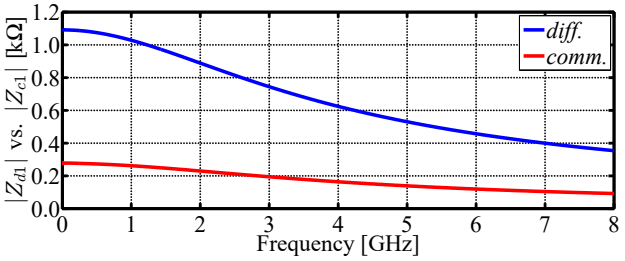

(a) Differential-mode and common-mode input impedance.

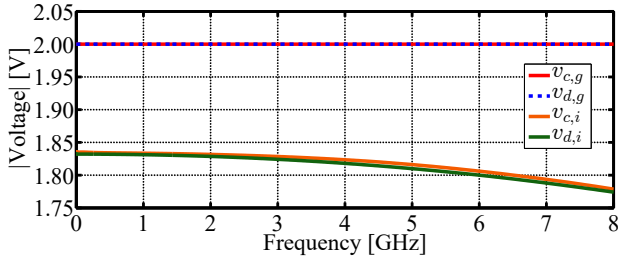

(b) Generator and input voltage.

Fig. 6. Probe circuit simulation results. The magnitude of the differential-mode input impedance Z_{d1} and the common-mode input impedance Z_{c1} are compared (top). The magnitude of the common-mode generator voltage $v_{c,g}$, the differential-mode generator voltage $v_{d,g}$, the common-mode input voltage $v_{c,i}$, and the differential-mode input voltage $v_{d,i}$ are compared (bottom).

probe circuit simulation setup are defined as follows:

$$v_{c,g} = v^+_{c,g} + v^-_{c,g}, \tag{2}$$

$$v_{d,g} = v^+_{d,g} - v^-_{d,g}. \tag{3}$$

The common-mode voltage at the input balanced logical port (P1) of the probe circuit $v_{c,i}$ and the differential-mode voltage at the input of the probe circuit $v_{d,i}$ in the probe circuit simulation setup are defined as follows:

$$v_{c,i} = v^+_{c,i} + v^-_{c,i}, \tag{4}$$

$$v_{d,i} = v^+_{d,i} - v^-_{d,i}. \tag{5}$$

The differential-mode input impedance Z_{d1} and the common-mode input impedance Z_{c1} of the simulated probe circuit at the balanced logical port (P1) are calculated [10]. The differential-mode input impedance Z_{d1} and the common-mode input impedance Z_{c1} of the simulated probe circuit are shown in Fig. 6(a). Both the differential-mode input impedance and the common-mode input impedance decrease with frequency, from the nominal value of 1092 Ω and 275 Ω, respectively. The impedances decrease to approximately 1/3 of the nominal value at 8 GHz, while the relative ratio between the two impedances remains around 4:1 in the entire frequency range. The drop in impedance at higher frequencies is a result of the attenuator circuit component and printed circuit board (PCB) parasitics. The input impedance of the probe circuit matches the input impedance of the attenuator structure very similarly, given that the input impedance of the laser, that is connected to the output of the attenuator, is matched to the 100 Ω differential-mode characteristic impedance.

The common-mode and differential-mode voltages at the generator and at the input of the simulated probe circuit are compared in Fig. 6(b). Given that the voltages of the individual generators are set to 1 V, both the differential-mode voltage at the generator $v_{d,g}$ and the common-mode voltage at the generator $v_{c,g}$ is fixed to 2 V. Both the differential-mode input voltage $v_{d,i}$ and the common-mode input voltage $v_{c,i}$ are close to the generator voltage of 2 V, given that both the differential-mode input impedance Z_{d1} and the common-mode input impedance Z_{c1} of the probe circuit are significantly higher than the generator differential-mode internal impedance of 100 Ω, and the generator common-mode internal impedance of 25 Ω. Both input voltages slightly decrease with frequency given that both the differential-mode and the common-mode input impedance decrease with frequency, while the internal impedance of the generator remains constant. Despite the common-mode input impedance being lower, the common-mode input voltage is slightly higher than the differential-mode input voltage, because the common-mode input impedance is higher relative to the 25 Ω generator common-mode internal impedance, than the differential-mode input impedance is relative to the 100 Ω generator differential-mode internal impedance.

B. Attenuator Signal Transmission

The mixed-mode S-parameter simulation results of the attenuator used in the probe circuit are shown in Fig. 7. Both the differential-to-differential transmission coefficient S_{dd21} and the common-to-common transmission coefficient S_{cc21} are very stable over the entire frequency range. The common-mode transmission coefficient is slightly higher than the differential-mode transmission

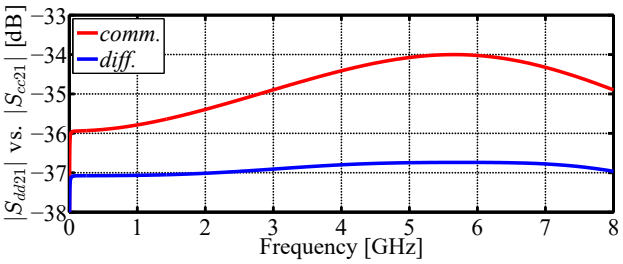

Fig. 7. EM simulations of the attenuator used in the probe circuit simulation. The magnitude of the differential-to-differential transmission coefficient S_{dd21} and the common-to-common transmission coefficient S_{cc21} are compared.

coefficient, meaning that the common-mode signal is less attenuated than the differential-mode signal. The mode conversion in the attenuator circuit EM simulations is limited. The mode conversion transmission coefficients S_{dc21} and S_{cd21} extracted from the simulation are significantly lower than it would be expected in practice. For this reason, the mode conversion in the attenuator circuit is not taken into account in this analysis.

C. Impedance Matching Between the Attenuator and the Laser

The differential-mode output impedance Z_{d2} and the common-mode output impedance Z_{c2} of the attenuator circuit are shown in Fig. 8(a). Both the differential-mode output impedance and the common-mode output impedance decrease with frequency, from the nominal value of 1092 Ω and 275 Ω, respectively. The impedances decrease to about 1/12 of the nominal value at 8 GHz,

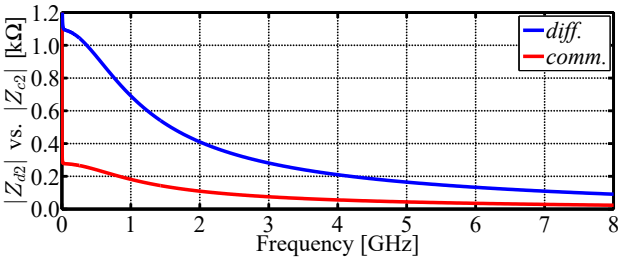

(a) Attenuator differential-mode and common-mode output impedance.

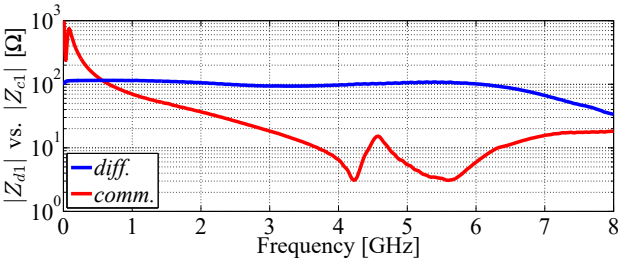

(b) Laser differential-mode and common-mode input impedance.

Fig. 8. Comparison of the EM simulations of the attenuator and the measurements of the laser used in the probe circuit simulation. The magnitude of the attenuator differential-mode output impedance Z_{d2} and the common-mode output impedance Z_{c2} are compared (top). The magnitude of the laser differential-mode input impedance Z_{d1} and the common-mode input impedance Z_{c1} are compared (bottom).

while the relative ratio between the two impedances remains around 4:1 in the entire frequency range. The output impedance of the attenuator circuit is lower than the input impedance in most of the frequency range.

The magnitude of the differential-mode input impedance Z_{d1} and the common-mode input impedance Z_{c1} of the measured laser diode is shown in Fig. 8(b). The differential-mode input impedance of the laser is matched to the 100 Ω differential-mode internal impedance of the generator. At frequencies above 6.1 GHz, the differential-mode input impedance drops off a bit. The common-mode input impedance of the laser is very high at lower frequencies and drops gradually, with the minimum around 4.2 GHz, followed by a resonance and an antiresonance. The common-mode input impedance increases for frequencies above 5.6 GHz, but remains lower than the differential-mode input impedance.

D. Laser Input Voltage

The voltage components at the input balanced logical port (P1) of the laser, for the differential-mode and common-mode characterization of the laser by itself are shown in Fig. 9(a). The voltage components at the input of the laser extracted from the probe circuit simulation (Fig. 3), where the laser is connected in cascade with the attenuator circuit, for the differential-mode and common-mode characterization are shown in Fig. 9(b). The common-mode input voltage component $v_{c,i,c}$ and the differential-mode input voltage component $v_{c,i,d}$ for the common-mode characterization are defined as follows:

$$v_{c,i,c} = v_{c,i}^{+} + v_{c,i}^{-}, \tag{6}$$

$$v_{c,i,d} = v_{c,i}^{+} - v_{c,i}^{-}. \tag{7}$$

The differential-mode input voltage component $v_{d,i,d}$ and the common-mode input voltage component $v_{d,i,c}$ for the differential-mode characterization are defined are defined as follows:

$$v_{d,i,d} = v_{d,i}^{+} - v_{d,i}^{-}, \tag{8}$$

$$v_{d,i,c} = v_{d,i}^{+} + v_{d,i}^{-}. \tag{9}$$

When the laser is characterized by itself, the differential-mode input voltage $v_{d,i,d}$ follows the trend of the differential-mode input impedance Z_{d1}, while the common-mode input voltage $v_{c,i,c}$ follows the trend of the common-mode input impedance Z_{c1} of the laser shown in Fig. 8(b). For the differential-mode characterization, the differential-mode signal component $v_{d,i,d}$ is around 1 V, because the differential-mode input impedance of the laser is matched to the 100 Ω generator differential-mode internal impedance. At frequencies above 6.1 GHz, the differential-mode voltage component drops with the differential-mode input impedance. For the common-mode characterization, the common-mode voltage component $v_{c,i,c}$ at low frequencies is around 2 V, because of the much higher common-mode input impedance of the laser compared to the 25 Ω generator common-mode internal

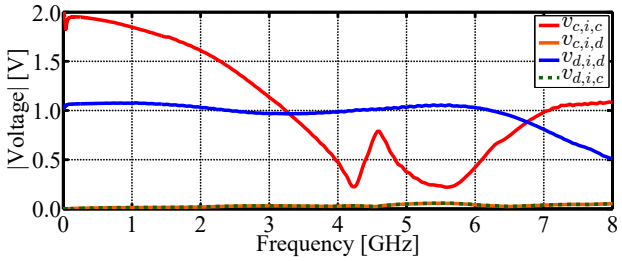

(a) Input voltage of the laser characterized by itself.

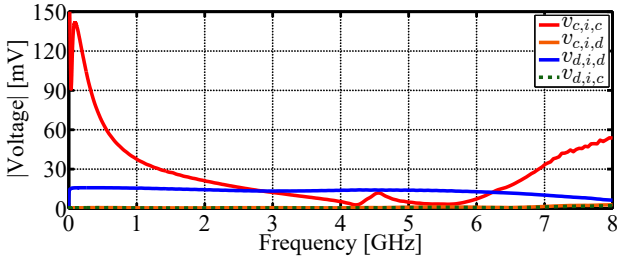

(b) Input voltage of the laser used in the cascade connection with the attenuator in the probe circuit simulation.

Fig. 9. Comparison of the voltage at the input of the laser diode extracted from the measurements of the laser by itself (top), and extracted from the probe circuit simulation using the cascade connection of the attenuator and the laser (bottom). The magnitude of the common-mode voltage component $v_{c,i,c}$ and the differential-mode voltage component $v_{c,i,d}$ in the common-mode characterization, and the differential-mode voltage component $v_{d,i,d}$ and the common-mode voltage component $v_{d,i,c}$ in the differential-mode characterization are compared.

impedance. At higher frequencies the common-mode voltage component decreases as a result of the changes in the common-mode input impedance. Due to the asymmetry of the laser, a differential-mode voltage component $v_{c,i,d}$ is present in the common-mode characterization, and a common-mode voltage component $v_{d,i,c}$ is present in the differential-mode characterization. These components slowly increase with frequency.

In the probe circuit, the laser is connected in cascade with the attenuator circuit (Fig. 3). The differential-mode and the common-mode voltage at the input of the laser are dependent on the attenuation of the differential-mode and the common-mode signal in the attenuator shown in Fig. 7, and the impedance matching between the output impedance of the attenuator and the input impedance of the laser shown in Fig. 8. More common-mode signal passes through the attenuator than the differential-mode signal. The differential-mode voltage $v_{d,i}$ and the common-mode voltage $v_{c,i}$ at the input of the probe circuit, shown in Fig. 6(b), are very similar and decrease very slightly with frequency, so this does not have a significant impact on the laser input voltage.

The common-mode output impedance Z_{c2} of the attenuator drops gradually with frequency, while the common-mode input impedance Z_{c1} of the laser drops quickly up to 4.2 GHz, but starts increasing again after 5.6 GHz. For the common-mode characterization the common-mode input voltage component $v_{c,i,c}$ roughly follows the trend of the common-mode input impedance of the laser. However, compared to the nominal case when the laser is characterized by itself, the common-mode input voltage $v_{c,i,c}$ is higher relative to the differential-mode input voltage $v_{d,i,d}$ in the lower frequency range up to 1.8 GHz and in the high frequency range above 5.5 GHz, while it is lower in the frequency range between 1.8 GHz and 4.2 GHz, as shown in Fig. 10.

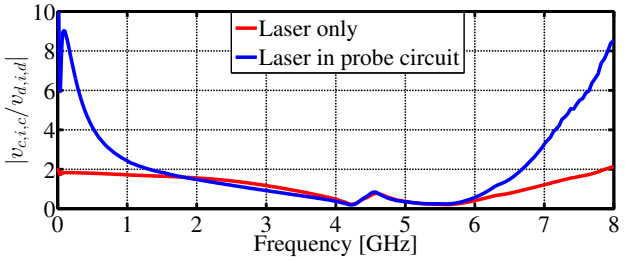

Fig. 10. Comparison of the voltage at the input of the laser extracted from the measurements of the laser by itself, and extracted from the probe circuit simulation using the cascade connection of the attenuator and the laser. The magnitude of the ratio of the common-mode voltage component in the common-mode characterization $v_{c,i,c}$ and the differential-mode voltage component in the differential-mode characterization $v_{d,i,d}$ is compared.

The differential-mode output impedance Z_{d2} of the attenuator drops gradually with frequency, while the differential-mode input impedance Z_{d1} of the laser remains almost constant up to 6.1 GHz. This means that more differential-mode voltage $v_{d,i,d}$ is applied at the input of the laser at lower frequencies, compared to the nominal case when the laser is characterized by itself.

E. Laser Signal Transmission

The mixed-mode S-parameter measurements of the laser used in the probe circuit simulation are shown in Fig. 11. The differential-mode transmission coefficient S_{sd21} is relatively stable over the entire frequency range. At frequencies above 6.6 GHz, there is a slight drop in the differential-mode signal level. The common-mode transmission coefficient S_{sc21} increases gradually with frequency over the measurement frequency range. The common-mode rejection ratio of the laser drops gradually with frequency, as shown in Fig. 12. It is above 30 dB up to 600 MHz and above 20 dB up to 3.1 GHz. It should be noted that the sudden drop in the CMRR above 4.5 GHz that is observed in the probe circuit characteristic is not

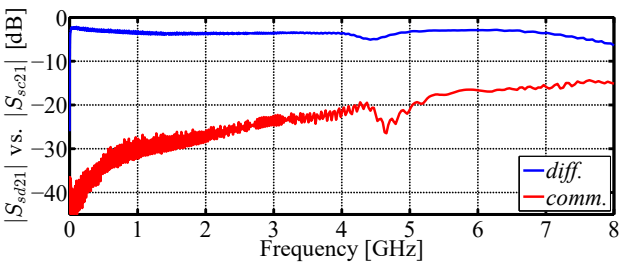

Fig. 11. Measurements of the laser used in the probe circuit simulation. The magnitude of the differential-mode transmission coefficient S_{sd21} and the common-mode transmission coefficient S_{sc21} are compared.

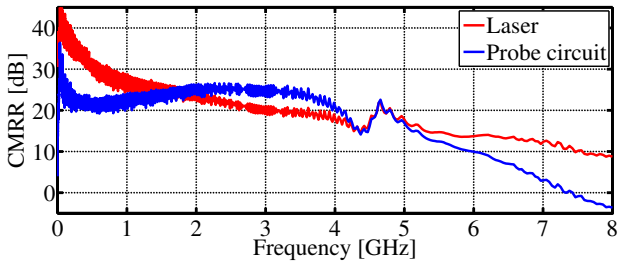

Fig. 12. Comparison of the common-mode rejection ratio (CMRR) of the probe circuit simulation and the measurement of the laser used in the probe circuit simulation.

present in the CMRR characteristic of the laser, nor the differential-mode and the common-mode characteristic. The same is true for the attenuator mixed-mode S-parameter characteristics shown in Fig. 7.

IV. Discussion

The high frequency drop in the CMRR that is observed in the probe circuit measurement and simulation results, shown in Fig. 4, is a result of the interaction between the attenuator circuit and the laser. Taking into account the differential-mode and common-mode signal propagation through the attenuator circuit, due to the impedance matching between the attenuator circuit and the laser, the common-mode voltage at the input of the laser increases significantly in the frequency range up to 1.8 GHz and above 4.2 GHz, relative to the differential-mode voltage, as shown in Fig. 10. Because of the higher common-mode signal relative to the differential-mode signal at the input of the laser, compared to the nominal case when the laser is characterized by itself, the CMRR of the probe circuit is degraded. The probe circuit CMRR is decreased in the frequency range up to 1.7 GHz and above 4.9 GHz. In turn, in the frequency range between 1.9 GHz and 4.3 GHz, where the common-mode signal is more attenuated than the differential-mode signal relative to the nominal case, the simulated probe circuit has a higher CMRR than the laser characterized by itself, as shown in Fig. 12.

The impedance matching between the attenuator circuit and the laser has a crucial effect on the CMRR characteristics of the probe circuit. In particular, the higher common-mode laser input voltage at lower frequencies, relative to the differential-mode input voltage, when compared to the characterization of the laser by itself, results in a relatively stable CMRR up to around 4 GHz. The typically higher CMRR of the laser at lower frequencies is flattened out by the higher common-mode voltage at the input of the laser, that is connected in cascade with the attenuator. Using the same mechanism, the increasing common-mode input voltage at high frequencies, relative to the differential-mode input voltage, when compared to the characterization of the laser by itself, accelerates the rate at which the CMRR drops at frequencies above 4.5 GHz, resulting in a steep slope.

A higher CMRR of the probe circuit could potentially be achieved by reducing the parasitic capacitance in the attenuator circuit and the laser diode layout, controlling the ground paths, and employing more effective common-mode signal filtering techniques.

V. Conclusion

An important mechanism of the common-mode signal propagation through the probe circuit is demonstrated. It is shown that not only the suppression of the common-mode signal and the mode conversion in each part of the probe circuit is important, but also the transmission of the differential-mode and the common-mode signal between the attenuator and the laser. While the CMRR of the probe circuit is primarily dependent on the CMRR of the laser used for the electro-optical conversion of the signal, the CMRR of the system can be increased above the CMRR of the laser, by optimizing the attenuator circuit design. The CMRR of the system can be improved by controlling the output impedance of the attenuator and the input impedance of the laser, where the portion of the common-mode signal that is transmitted to the laser should be minimized, while achieving a high transmission of the differential-mode signal.

Acknowledgment

This work was supported in part by the Croatian Science Foundation (HRZZ) within the project Fast switching converters based on GaN devices and resonant architectures (IP-2019-04-8959).

References

[1] H. Štimac, "Design and characterization of multiport electro-optical circuits for broadband voltage measurements in an electromagnetically polluted environment," Ph.D. dissertation, University of Zagreb Faculty of Electrical Engineering and Computing, 2020.

[2] H. Štimac, R. Gillon, and A. Barić, "Common-mode rejection ratio characterisation of a broadband electro-optical differential esd voltage probe," *Electronics Letters*, vol. 55, no. 19, pp. 1047–1049, Sep 2019.

[3] G. Colman, J. Bauwelinck, R. Gillon, A. Wieers, and J. Vandewege, "Wideband measurement system for on-chip esd waveform characterisation," *Electronics Letters*, vol. 48, no. 3, pp. 150–152, February 2012.

[4] Chong Ding and D. Pommerenke, "Laser optical in-circuit measurement system for immunity applications," in *2006 IEEE International Symposium on Electromagnetic Compatibility, 2006. EMC 2006.*, vol. 3, Aug 2006, pp. 569–574.

[5] *R&S ZVB Vector Network Analyzer Specifications*, Rohde & Schwarz GmbH & Co. KG, June 2011. [Online]. Available: https://scdn.rohde-schwarz.com/ur/pws/dl_downloads/dl_common_library/dl_brochures_and_datasheets/pdf_1/ZVB_dat_sw_en.pdf

[6] *Application Note: Three and Four Port S-parameter Measurements*, Anritsu, May 2002. [Online]. Available: http://ytdp.ee.wits.ac.za/11410-00279B.pdf

[7] K. Jung, L. A. Hayden, O. D. Crisalle, W. R. Eisenstadt, R. M. Fox, P. Hanaway, R. L. Campbell, C. McCuen, and M. Lewis, "A new characterization and calibration method for 3-db-coupled on-wafer measurements," *IEEE Transactions on Microwave Theory and Techniques*, vol. 56, no. 5, pp. 1193–1200, May 2008.

[8] W. Eisenstadt, *Microwave differential circuit design using mixed-mode S-parameters*. Boston: Artech House, 2006.

[9] *Keysight EEsof EDA EMPro*, Keysight Technologies, Inc., Sep 2017. [Online]. Available: https://www.keysight.com/us/en/assets/7018-02343/brochures/5990-4819.pdf

[10] C. T. Carrasco, C. J. Sieiro, J. M. Lopez-Villegas, N. Vidal, R. R. Gonzalez-Echevarría, and M. E. Roca, "Mixed-mode impedance and reflection coefficient of two-port devices," *Progress In Electromagnetics Research*, vol. 130, pp. 411–428, 2012.